

ORIGINAL ARTICLE

Open Access



Establishment and characterization of a canine chondrosarcoma cell line: Mango

Meilin Wang¹, Xiao Wang¹, Lixin He¹, Hongbo Gao¹, Wenxuan Li¹, Huili Feng¹, Qingyuan Zhao¹, Wenwen Zhang¹, Chengzong Li¹, Bohan Zhang¹ and Changwei Qiu^{1*}

Abstract

In the global progress of bone tumor research, established stable and long-lasting transgenic chondrosarcoma (CSA) cell lines are rare, mainly of murine and human origin, while the establishment of canine CSA cell lines has yet to be reported. This study established a canine CSA cell line to facilitate the basic clinical study of canine CSA. Fifty five cases of canine osteolytic disease were collected, and more than 10 bone tumor samples from dogs with typical clinical signs were used for primary cell culture. A cell line with stable passaging for more than 100 generations and mouse tumorigenic ability was successfully cultured. According to the clinical characteristics of the dog and the histopathological results of the primary tumor, CSA was diagnosed, and the CSA cell line was designated Mango. Immunohistochemical (IHC) results showed that the immunoreactivity of bone gamma-carboxyglutamate protein (BGLAP), secreted protein acidic and rich in cysteine (SPARC), alkaline phosphatase (ALPL), vimentin (VIM) and S100 were positive. However, the immunoreactivity of pan-cytokeratin (PCK), chromogranin A (CGA), and platelet endothelial cell adhesion molecule-1 (CD31) was negative. Immunofluorescence (IF) results showed that the protein expressions in the Mango cell line were consistent with the IHC identification of the primary tumor. The Mango cell line's doubling time was 43.92 h, and the cell formation rate exceeded 20%. There were abnormal chromosome numbers, hetero staining with toluidine blue, and certain calcification abilities. It could be passaged stably and continuously without changing the cell morphology and characteristics. In vivo, the cells were successfully injected into the nude mice model with a tumorigenic rate of 100%. The immunophenotype of the xenograft tumor was consistent with that of the primary tumor. Therefore, we effectively established a canine CSA cell line. As a promising cell material, this cell line can be used to construct a tumor-bearing model conducive to the subsequent basic research of canine CSA. Moreover, because of its similarity to human CSA, the animal model of CSA is also indispensable for investigating human CSA.

Keywords Canine chondrosarcoma, Cell line, Establishment, Characterization, Tumorigenicity

Introduction

Canine chondrosarcoma(CSA) is a malignant cartilaginous-derived tumor with multiple morphologic features and clinical manifestations that is insensitive to both

chemotherapy and radiotherapy, and the main treatment modality nowadays is extensive resection of the affected area (Monderer et al. 2013; Whelan and Davis 2018; Tlemsani et al. 2023). In a retrospective study by the Veterinary Society for Surgical Oncology (VSSO), the scaphorectomy of 42 dogs with scaphoid tumors of varying degrees of severity resulted in effective treatment, and most dogs did not have any problems with limb use after surgery (Montinaro et al. 2013).

*Correspondence:

Changwei Qiu
sdqiu2001@mail.hzau.edu.cn

¹ Department of Clinical Veterinary Medicine, College of Veterinary Medicine, Huazhong Agricultural University, Wuhan 430070, China



© The Author(s) 2023. **Open Access** This article is licensed under a Creative Commons Attribution 4.0 International License, which permits use, sharing, adaptation, distribution and reproduction in any medium or format, as long as you give appropriate credit to the original author(s) and the source, provide a link to the Creative Commons licence, and indicate if changes were made. The images or other third party material in this article are included in the article's Creative Commons licence, unless indicated otherwise in a credit line to the material. If material is not included in the article's Creative Commons licence and your intended use is not permitted by statutory regulation or exceeds the permitted use, you will need to obtain permission directly from the copyright holder. To view a copy of this licence, visit <http://creativecommons.org/licenses/by/4.0/>. The Creative Commons Public Domain Dedication waiver (<http://creativecommons.org/publicdomain/zero/1.0/>) applies to the data made available in this article, unless otherwise stated in a credit line to the data.

However, despite the use of surgical resection, treatment effects are still not satisfactory. In another retrospective study by the VSSO, in which 25 canine CSA of the extremities were analyzed, CSAs originating from the extremities could be effectively treated by amputation alone. Low to intermediate-grade CSAs have a good prognosis, while high-grade tumors present aggressively (Farese et al. 2009). The management of CSA remains an ongoing challenge, and conventional chemotherapeutic agents targeting the DNA machinery, such as docetaxel, paclitaxel, and cisplatin, are ineffective (Van Oosterwijk et al. 2013). New therapeutic approaches, such as immunotherapy or new molecular targeting agents, are needed to improve the clinical outcome of animals with CSA (Miwa et al. 2022). However, few studies have examined the potential clinical application or translation of immunotherapies in dogs (Poon et al. 2020).

Canine bone-derived tumors are highly prevalent, have similar biological behavior, molecular profile, and micro-environment compared to human bone tumors, and are more susceptible to larger body sizes (Morello et al. 2011). The short natural life span of dogs and the more rapid progression and metastasis of cancer compared to human patients allow for more rapid clinical trials in this species. This animal model is clinically similar to human CSA and is considered an indispensable tool to explore the pathogenesis, metastasis, and drug resistance mechanisms of CSA or to evaluate the therapeutic efficacy of new therapies (Liao et al. 2013; Al-Khan et al. 2017).

This study aims to establish a canine CSA cell line, characterize its morphology, proliferation, chromosomal characteristics, immunophenotype, and tumorigenicity, and provide good cellular material for subsequent identification of potential molecular biomarkers, establishing animal models, and screening of potential cancer therapies. Furthermore, the canine CSA cell line could also be applied to investigate further the etiology, metastasis mechanism, drug resistance mechanism, and clinical intervention of the CSA.

Results

The outcome and assessment of a 10-year-old male castrated golden retriever

The affected dog exhibited distinctive clinical characteristics, including rapid disease progression, lameness in the left forelimb, and a hard, swollen, and ill-defined border around the shoulder joint upon palpation. Computed tomography (CT) examination revealed diffuse osteolysis and hyperplasia in the affected dog's left scapula and proximal humerus (Fig. 1A and B, row), with no distal organ metastases seen for the time being. Puncture of the

diseased area was performed, and fine needle aspiration (FNA) revealed a large number of erythrocytes, inflammatory cells, mesenchymal cells (Fig. 1C, dotted arrow) (2–4 cells per 400×), and occasional osteoclasts (Fig. 1C, red arrow) and osteoblasts (Fig. 1C, black arrow).

Tumor tissues were sterilely surgically removed from the left scapula of the dog in an animal hospital. The dog was amputated following standard operating procedures and with the consent of the pet owner. The tumor tissue resembled hyaline cartilage with a smooth, translucent, off-white, moderately hard surface poorly demarcated from normal bone tissue. The dog did not receive pre-operative chemotherapy or radiotherapy. The case was highly consistent with the clinical features of malignant bone tumors in dogs, and after surgical excision, tumor samples were immediately processed for cell culture and histopathological confirmation. A portion of the tissue was embedded in paraffin, and the diagnosis was confirmed by histology and IHC.

After amputation, the dog was treated with conventional chemotherapeutic agents, such as cisplatin, and returned six months later with good mental status and no recurrence. Based on previously published diagnostic features of CSA in dogs, the histopathology report confirmed the diagnosis of CSA by hematoxylin-eosin (H&E) staining analysis. On section, the cartilage was disorganized with bone, and there were multiple adjacent well-differentiated but disorganized hyaline cartilage lobules (Fig. 1D). Under high magnification, the tumor cells were heterogeneous with variable cell size, distinct nuclei, and visible nuclear division phase. The bone trabeculae were infiltrated by disorganized malignant chondrocytes (Fig. 1E), and the trabeculae in contact with cartilage were likely formed by endochondral ossification. Purplish-red calcium salt deposits around some tumor cells (Fig. 1F, arrow) indicated peri-tumor cell calcification. The tumor giant cells within the vessels (Fig. 1G, arrow) indicated that the tumor has metastasized. Masson staining revealed many collagen fibers staining blue, mature or pre-existing bone staining red, and tumor-like neoplastic bone predominantly blue with small central areas of red (Fig. 1H). Therefore, this canine CSA was classified as a conventional CSA with grade III in histological grading.

Establishment of the Mango cell line

Fresh bone tumor samples were obtained under aseptic manipulation with the consent of the pet owner. The tumor tissues were digested with neutral protease and III-collagenase, and some of the cells were seen to adhere to the bottom wall of culture flasks after 72 h (Fig. 2A).

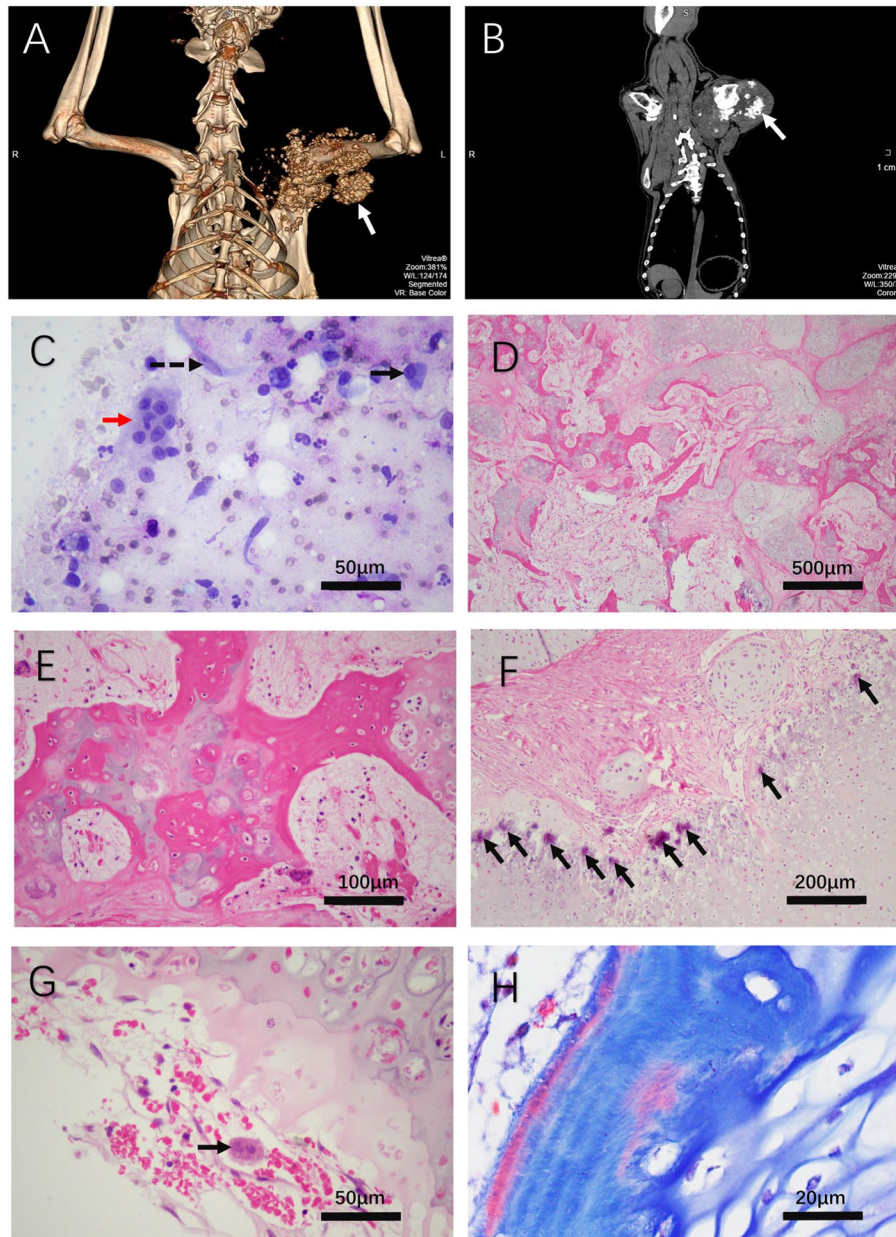


Fig. 1 Clinical features and pathological analysis of the affected dogs. **A** CT 3D reconstruction, dorsoventral position. **B** CT, coronal plane. **C** Cytological findings, diff-quick staining. Mesenchymal cells (dotted arrow), occasional osteoclasts (red arrow) and osteoblasts (black arrow). **D** H&E staining. **E** H&E staining. **F** H&E staining. The arrow refers to purplish-red calcium salt deposits around some tumor cells. **G** H&E staining. The arrow refers to tumor giant cell. **H** Masson staining of tumor tissue

We successfully purified and stably passed a canine CSA cell line which was named after the affected dog, the Mango cell line.

Microscopic morphology of Mango cells

Under microscopy, Mango cells were morphologically arranged in a fibroblast-like pattern, with cells growing in a single layer against the wall, polygonal or

spindle-shaped, with large, eccentric nuclei, multiple nucleoli, clearly visible nuclear membrane and nucleoli, and abundant cytoplasm. The malignant multinucleated cells could be observed (Fig. 2B, arrow). Ultrastructure showed that Mango cells had well-developed Golgi apparatus (Fig. 2C, black arrow), abundant rough endoplasmic reticulum, more lysosomes (Fig. 2C, red arrow), and few mitochondria in the cytoplasm.

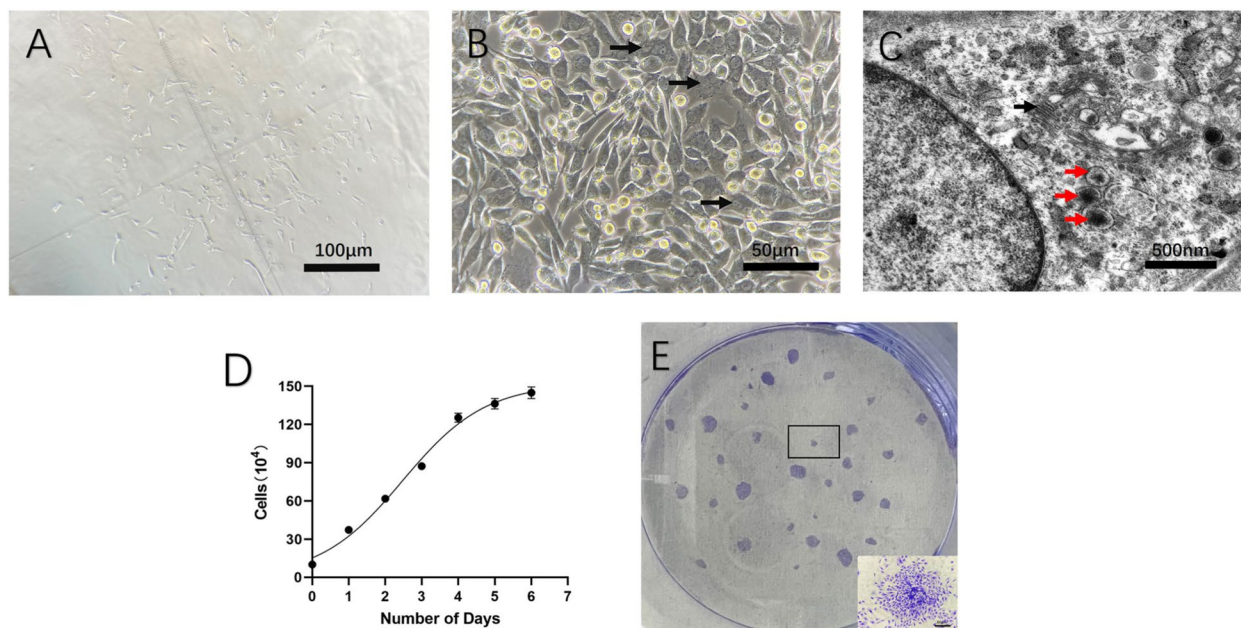


Fig. 2 Cell morphology and growth characteristics. **A** Microscopy, primary cells were apposed at 72 h. **B** Cell morphology in T-25 cm² culture flask, and the malignant multinucleated cells could be observed (arrow). **C** Cell ultrastructure. Well-developed Golgi apparatus (black arrow) and multiple lysosomes (red arrow) are in the cytoplasm. **D** Cell growth curve; **E** Cell clone

Growth of the cells

The Mango cell line exhibited an “S-shaped” growth curve, as shown in Fig. 2D, and entered the plateau phase at d 5. The cell proliferation time was calculated by taking the data of the logarithmic growth period of d 1–4. The calculated cell proliferation time was 43.92 h. The cells grew well after cryopreservation. Large colonies of the cells were formed (20–30 colonies) at 2 weeks after a single cell suspension was planned, and the clone formation rate exceeded 20% (Fig. 2E).

Cytogenetic analyses

We chose 50 cells with reasonably long and evenly distributed chromosomes for observation and analysis (Fig. 3A). The typical number of chromosomes in dogs

was 78; however, in this cell line, the number of chromosomes ranged from 105 to 220, with a median of 119.5. The numbers of chromosomes were all over 78, and no integer ploidy variation of chromosomes was widespread (Fig. 3B).

Cell-specific staining

Alizarin red staining allowed observation of trace calcium salt deposits in the cells. Mango cells showed a faint red stain with orange-red calcium salt deposits under the microscope (Fig. 4A). The chondrocytes showed an obvious blue hetero-staining reaction to toluidine blue. In contrast, this cell line showed a blue cytoplasm with a large number of vacuoles, a darkly stained nucleus, a pyknotic or polygonal cell morphology, and blue-purple

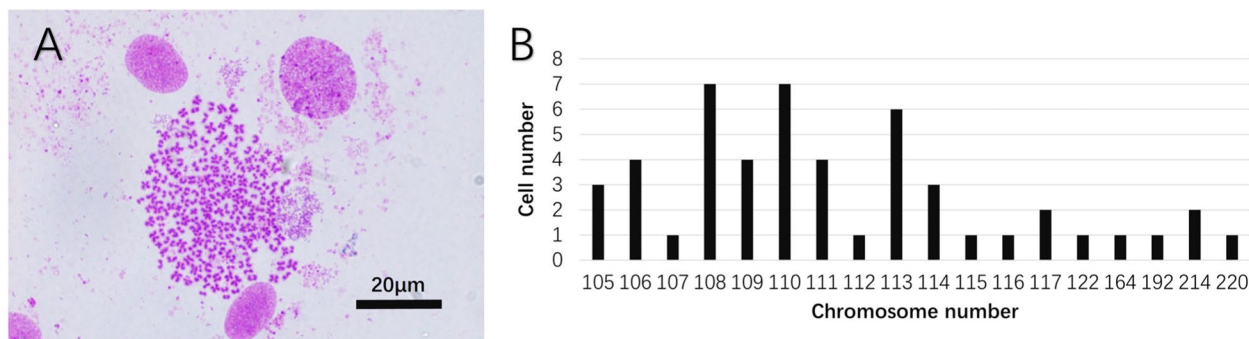


Fig. 3 Cell chromosome analysis. **A** Mid-division chromosome of a single cell. **B** Distribution of cell chromosome numbers

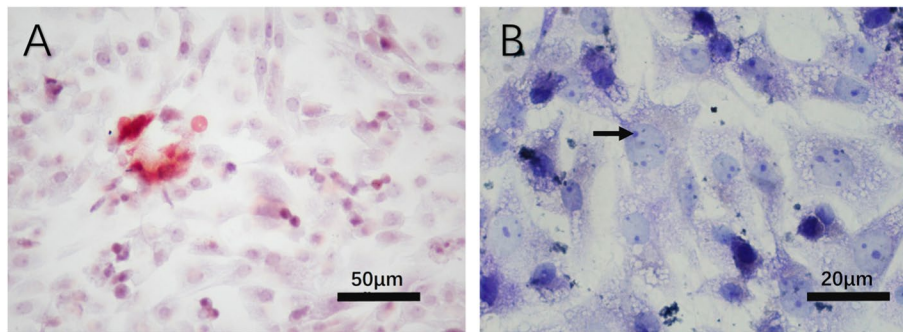


Fig. 4 Special staining of Mango cell line. **A** Alizarin red staining. **B** Toluidine blue staining

hetero-staining granules in the nucleus (Fig. 4B, arrow), which were aminoglycans secreted by chondrocytes.

Immunohistochemical characterization of the primary tumor

Immunohistochemical (IHC) methods were applied to detect the expression of bone gamma-carboxyglutamate protein (BGLAP), secreted protein acidic and rich in cysteine (SPARC), alkaline phosphatase (ALPL), vimentin (VIM), pan-cytokeratin (PCK), chromogranin A (CGA) and platelet endothelial cell adhesion molecule-1 (CD31) in the primary tumor. In this experiment, the negative control without a primary antibody was used. The results of the IHC analysis showed (Fig. 5) that BGLAP, SPARC,

and ALPL were weakly positive, S100 and VIM showed strong positive reactions, and CGA, PCK, and CD31 were negatively expressed.

Immunofluorescence characterization of Mango cell line

The expression of BGLAP, SPARC, ALPL, VIM, PCK, CD31, CGA, and S100 in Mango cells was detected by immunofluorescence (IF). In this experiment, the negative control without a primary antibody was used. The IF results showed (Fig. 6) that BGLAP, SPARC, ALPL, and VIM were cytoplasm positive, both the nucleus and cytoplasm of S100 showed positive, and CGA, PCK, and CD31 lacked expression. The results indicated that the Mango cell line exhibited an immune response similar to the primary canine CSA.

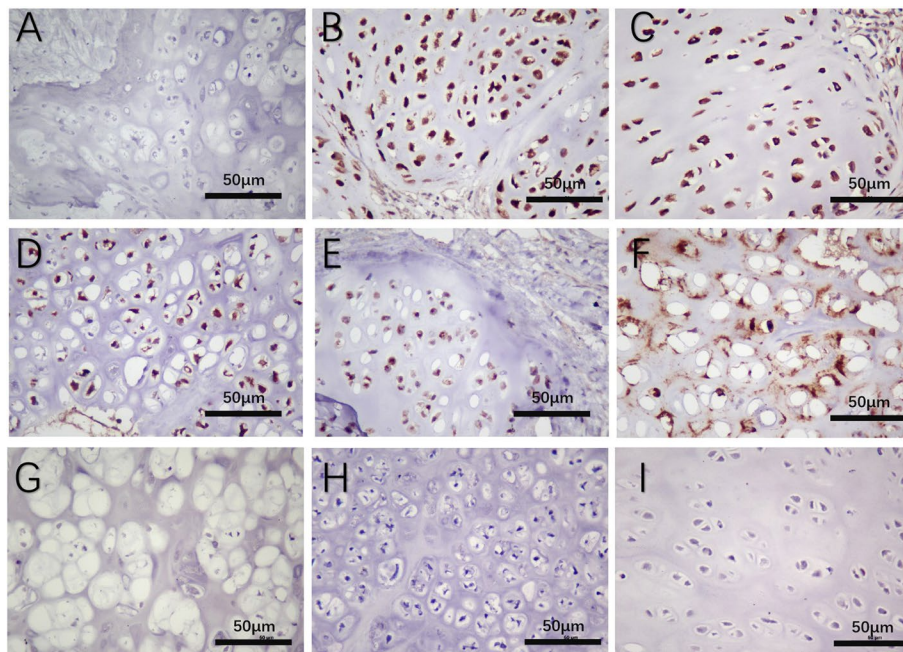


Fig. 5 IHC of primary tumor tissue (400 \times). Positive staining is dark brown, and **A** is the negative control. The primary tumor tissues were strongly positive for VIM (**C**) and S100 (**B**) in the nucleus, weakly positive for BGLAP (**D**) and SPARC (**E**) in the nucleus, weakly positive for ALPL (**F**) in the cytoplasm, and negative for CGA (**G**), CD31 (**H**) and PCK (**I**)

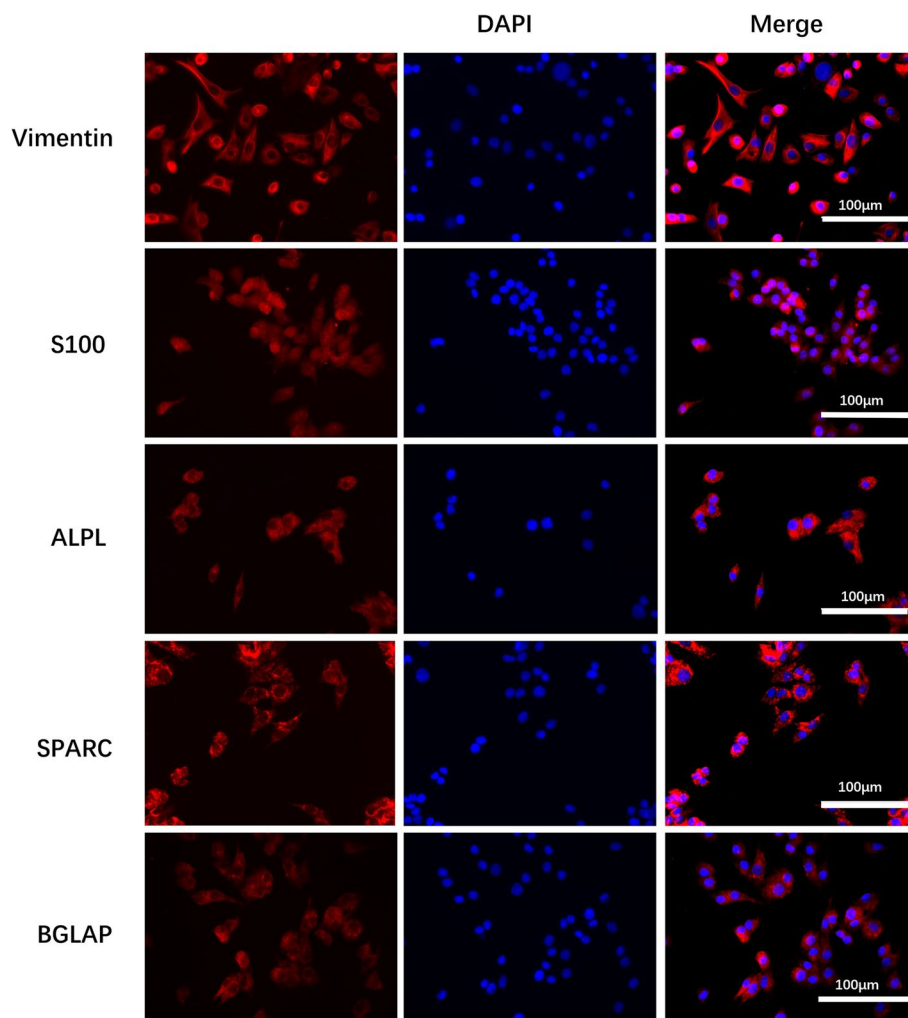


Fig. 6 IF of Mango cell line

Tumorigenesis and metastasis potentials of Mango cells in mice

Tumor growth was detected at all transplantation sites in mice (Fig. 7A, arrow). On d 14 of injection, there was significant angiogenesis in the dorsal tumors of nude mice (Fig. 7B, arrow). Every 2–3 d, mice were monitored for changes in body weight and tumors (Fig. 7C, D). The body weight of mice was stable and maintained between 23–24 g, and the maximum diameter of tumor was less than 15 mm, and the size of tumor was much less than 2000 mm³, which met the requirements of animal welfare. Mice were euthanized by cervical dislocation on d 23 after inoculation, and tumors in all mice were histologically confirmed as CSA. The histopathological morphology of the tumors in nude mice was similar to that of the primary tumor, with a lobulated structure consisting mainly of chondrocytes and stroma, disorganized arrangement, variable nuclei size, strong heterogeneity,

visible tumor giant cells (Fig. 7E, arrow), infiltration of tumor cells into surrounding tissues (Fig. 7F, arrow), and a high degree of malignancy. Due to the short experimental period, no obvious lesions on the lung or liver were observed for the time being.

Phenotypic identification of xenograft tumors

IHC was performed on the transplanted tumor in nude mice, and the results showed that the tumor tissue's immunophenotype was consistent with that of the primary tumor and the Mango cell line. BGLAP, SPARC, ALPL, S100, and VIM were positive. Still, PCK, CD31, and CGA were negative (Fig. 8). The successful establishment of the nude mouse model and the immunophenotype identification of the tumor demonstrated that the tumor originated from the Mango cell line. It maintained the good invasiveness and immunogenicity of the primary tumor during the cell culture.

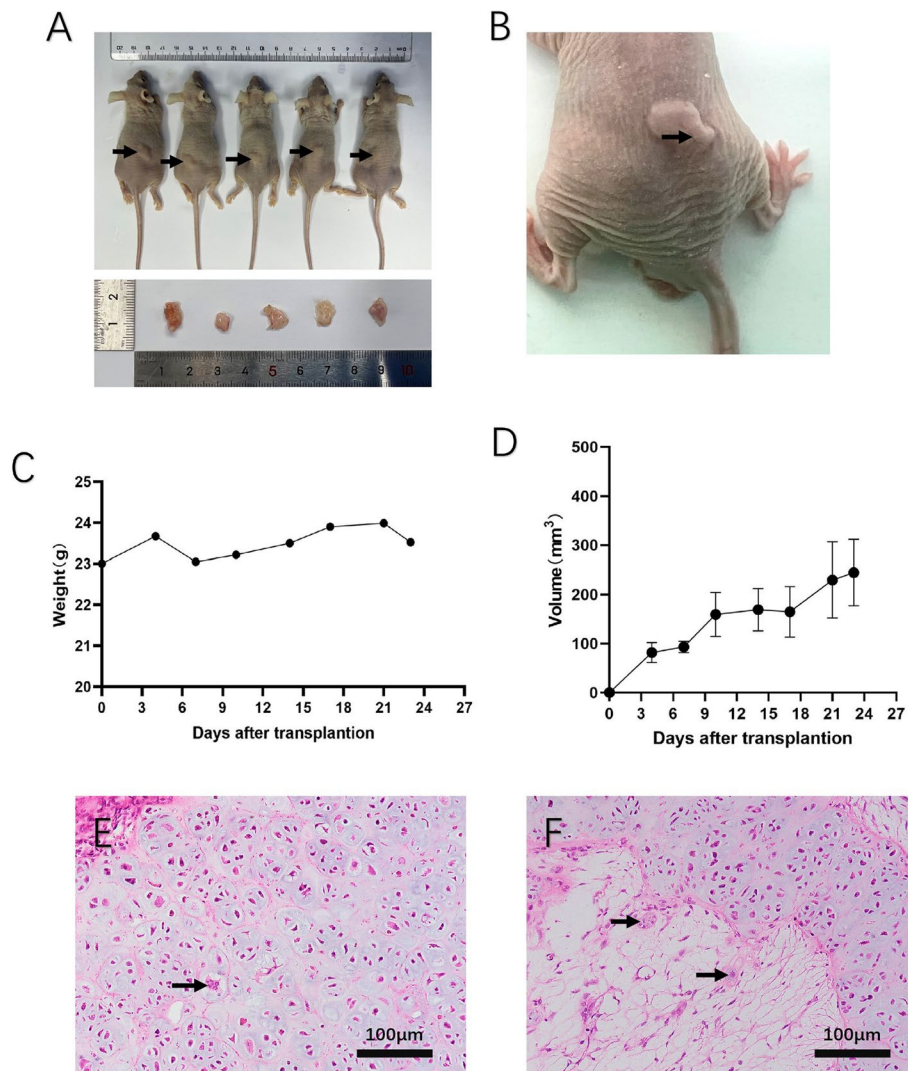


Fig. 7 Results of tumor-bearing experiments in nude mice. **A** Tumor-bearing nude mice with transplanted tumors. **B** Obvious angiogenesis on tumors. **C** Table of weight change in nude mice. **D** Growth curve of tumors in nude mice. **E, F** H&E stained sections of transplanted tumors. The arrow refers to tumor giant cells (**E**) and tumor cells infiltrated the surrounding normal tissue (**F**)

Discussion

Malignant bone tumors can be classified as osteosarcoma (OSA), CSA, and fibrosarcoma, and among several species, OSA is the predominant bone malignancy, followed by CSA (Al-Khan et al. 2017; Rizzo et al. 2017; Vinayak et al. 2018). The clinical manifestations of malignant bone tumors in dogs are all approximately the same, commonly occurring in large dogs, and if they occur in the extremities, the dog is lame in the affected limb, and the diseased area is swollen and hard to palpation. In diagnosing the disease, irregular hypodense shadows in the bone, known as osteolysis, are often detected on radiograph and CT. CT and magnetic resonance imaging (MRI) are good tools for assessing the

microscopic extent of bone tumors in dogs (Davis et al. 2002; Vanel et al. 2013; Engel et al. 2021).

During pet treatments, FNA can provide initial discrimination of the nature of bone tumors and observe the presence of malignant mesenchymal cells, but it is also often the case that the depth of the lesion makes this technique inextensible and limits diagnostic accuracy. Histopathologically, the OSA and CSA are also similar, and particular attention should be paid to differentiating chondroblasts' OSA from the CSA. IHC does not help diagnose OSA due to the lack of highly specific osteoblastic markers (Séguin et al. 2006). OSA is often more malignant, aggressive, and metastatic than CSA, with a poor prognosis.

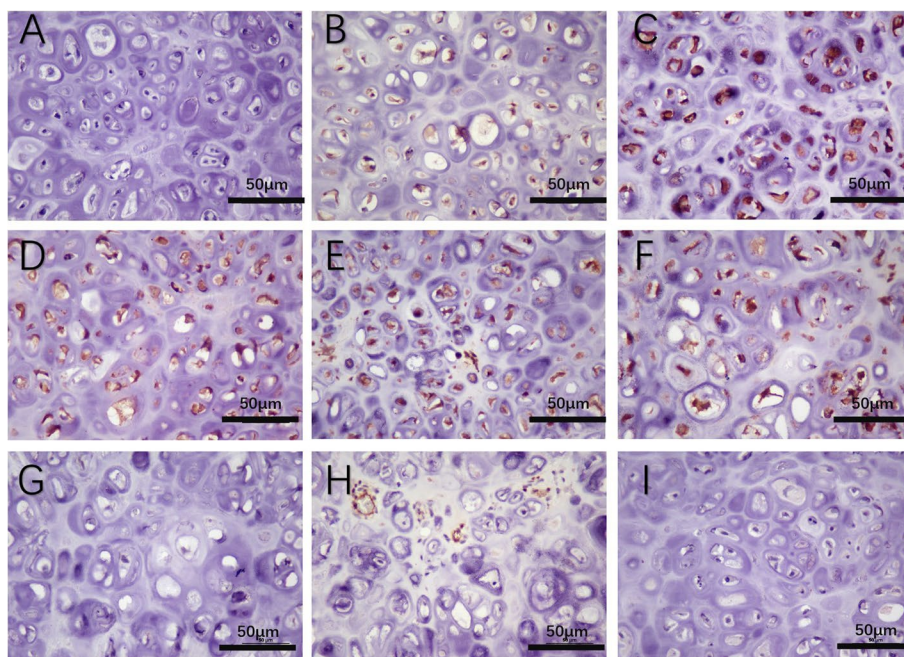


Fig. 8 IHC of transplanted tumors. Positive staining is dark brown, and **A** is the negative control. The tumor tissues of nude mice were positive for VIM (**C**), BGLAP (**D**), SPARC (**E**), ALPL (**F**), and S100 (**B**) but negative for PCK (**I**), CGA (**G**), and CD31 (**H**)

Relatively uniform clusters of chondrocytes are typical of many CSA, and the absence of mitotic signs or cytologic anisotropy does not exclude malignancy. Because the histologic appearance can vary markedly in different areas of the same tumor, and the core biopsy samples typically used for routine diagnosis cannot be considered representative of the entire lesion, there is no histologic grading system that has gained widespread use by veterinary pathologists. A grading system for CSA in dogs can refer to human grading criteria, with grade I chondrosarcoma showing low cell density with a cartilage-like stroma and no mitosis, grade II chondrosarcoma with mitosis present, and grade III chondrosarcoma, high cell density with mucus-like stromal changes and large nuclear heterogeneity (Chikata et al. 2006; Gelderblom et al. 2008; Van Oosterwijk et al. 2013).

Cultured cell lines are essential to study the molecular and cellular mechanisms of tumorigenesis and to establish animal models subsequently (Liu et al. 2016), and we urgently need suitable in vitro cell models to support clinical and basic research in canine CSA. Cellular models can assess the possible impact of new antitumor drugs and gene function by detecting phenotypic changes after drug treatment or gene transfection, respectively (Kito et al. 2018; Zu et al. 2022). Moreover, spontaneous tumors in dogs can often serve as a model for the biology and translational treatment of human cancers, with

a higher similarity to many existing experimental tumor models.

During the culture of the primary cell line, some malignant tumors can be naturally purified to grow single cell lines that maintain their characteristics in vivo better than normal cells to achieve immortality (Meyer and Walter 2016), and the Mango cell line fits this profile. Mango cell line grows slowly when first attached, with passages every 5 d for the first ten generations, and after adaptation to in vitro culture, they can be passaged every 2–3 d at the ratio of 1:2. The Mango cell line was found to be consistent with chondrogenic cell markers by toluidine blue staining, IF and calcium salt deposition ability analysis, and remained stable in cell morphology after multiple passages, with considerable diversity in chromosomal karyotypes, consistent with malignant tumor traits.

Chromosomal aneuploidy is exceptionally common in cancer cells. Cell diversity increases and mutated cancer cells can better adapt to different living environments. It has been suggested that chromosomal aneuploidy increases with tumor progression in many cancers, including the CSA, which may signal a transition from localized to aggressive disease. The chromosomal abnormalities in sarcomas are more frequent than those in common chondromas. Genetic aberrations increase as CSA progresses from low to high grades (Kim et al. 2011).

The Mango cell line was aggressive and malignant. It retained the immunological characteristics of the original CSA and was successfully transplanted into nude mice, and solid tumors were palpable by d 4 of injection. The tumor tissue showed significant angiogenesis, and H&E staining showed that it was consistent with the histological features of the primary tumor, with strong heterogeneity of tumor cells and infiltration into the surrounding tissues.

In the protein expression of the bone-derived tumor tissue or cells, ALPL is a marker of osteoblast bioactivation but is expressed in most CSA and is frequently expressed in III grade CSA. The positive rate of ALPL in different grades of CSA varies significantly and can be used as a prognostic reference. The significance of SPARC expression in CSA is unclear and is not limited to bone tissue. BGLAP, a bone-specific protein produced by osteoblasts with high specificity for bone-derived tumors, used to verify the tumor type and bone origin of Mango cell lines, was detected in approximately 70% of CSA, similar to previous human and veterinary reports (Lee and Tung 2013; Wehrle-Martinez et al. 2016), and can also be used as a prognostic in indicators (Fanburg et al. 1997). S100 is frequently expressed in malignant tumors and chondrocytes (Madarama et al. 1998). In addition to identifying the mesenchymal origin, elevated expression of VIM in canine bone tumors may be associated with an epithelial-mesenchymal transition leading to a more aggressive tumor phenotype and metastatic development (Amaral et al. 2018).

IHC staining of the primary tumor confirmed its mesenchymal origin (VIM positive), excluded tumors of carcinoma (PCK negative), vascular endothelial origin (CD31 negative), and neurogenic origin (CGA negative), and combined with histopathological features, determined its cartilaginous origin (SPARC, ALPL, BGLAP positive, S100 positive).

There are few studies on canine CSA, and there is no specific study on the immune microenvironment of canine CSA. In human medicine, the CSA has demonstrated CD163 macrophage infiltration, which has been associated with more invasive and higher-grade chondrosarcomas, while higher concentrations of CD8 T cells have been shown to repress chondrosarcoma progression (T-taylor et al. 2021). Due to the similarity between canine CSA and human CSA, these conclusions have certain reference significance in canine.

Conclusion

In this study, a canine CSA cell line, the Mango cell line, was successfully established. It can be continuously cultured in vitro while maintaining the characteristics of canine CSA cells and is 100% tumorigenic in nude mice,

making it suitable for establishing in vivo and in vitro animal models, which may contribute to the further exploration of diagnostic markers, related immunotherapy and drug development for canine CSA.

Materials and methods

Tumor specimens

From 2021 to 2023, the canine osteolytic cases in the animal hospital of Huazhong Agricultural University were collected. The basic information of the dogs, past medical history, clinical symptoms, and onset time, combined with interrogation, inspection, palpation, hematological examination, cytological examination, and reasonable use of imaging equipment, preliminary screening of dogs with bone tumors was performed. Dogs with clinical features or osteolytic images could be included in the case for further investigation. The radiograph, CT, and MRI images were collected. For osteolytic cases caused by bone tumors, amputation or tumor reduction surgery was performed with the consent of the pet owners, and tumor samples were obtained. A portion of the sterile tumor tissue was washed and transferred to an ultra-clean table to remove connective tissue and necrotic tissue, and a 1 cm³ size tissue was selected at the junction of the tumor and healthy tissue. The remaining tissues could be fixed in 4% paraformaldehyde fixative, and the volume ratio of tissue block to fixative solution was 1:10–1:20.

Cell line establishment and purification

The tumor tissues were washed with Hanks' Balanced Salt Solution (HBSS, Biosharp, Labgic) with 5% penicillin–streptomycin–amphotericin solution (Gibco, Life Technologies), and minced into 1 mm³ pieces, removing blood, fat, and fibroconnective tissues. Then, the tumor fragments were disaggregated with collagenase type III (Gibco, Life Technologies) and neutral protease (Gibco, Life Technologies) at 37°C in a humidified atmosphere of 5% CO₂ for 3–4 h with continuous agitation. After that, the digested tissue was filtered through nylon mesh cloth (100 μm) and centrifuged at 1000 rpm for 5 min, and the pelleted cells were resuspended in Dulbecco's modified Eagle's medium (DMEM, Gibco, Life Technologies) containing 15% fetal bovine serum (FBS, Hyczymbio, Wuhan, China) and 1% penicillin–streptomycin solution (Gibco, Life Technologies). The cell suspension was placed in a 25 cm² cell culture flask (NEST Biotechnology, Wuxi) and maintained in a humidified atmosphere of 5% carbon dioxide at 37 °C. Cell culture was observed daily by phase-contrast microscopy.

After forming a complete monolayer in the primary culture, cells were transferred into a new flask with fresh DMEM-15% FBS medium. Once the cell cultures were 80–90% confluent, the cells were washed with phosphate-buffered saline (PBS), treated with 0.25% trypsin solution (Gibco, Life Technologies), incubated until they dislodged from the flask surface, and split at a ratio of 1:2 in fresh DMEM-15% FBS medium. Additionally, the cells were sampled and frozen every two passages.

Electron microscopy

Cells were spread in six-well plates, and when growth reached 70–80% confluence, the medium was discarded, 2.5% glutaraldehyde electron microscopy fixative was added and held at room temperature (RT) for 2 h. Cells were gently scraped off with a cell scraper and collected into centrifuge tubes, cells were centrifuged to the bottom of the tubes, and the precipitate was visible to the

$$\text{Clone formation rate} = (\text{number of clones}/\text{number of inoculated cells}) \times 100\%.$$

naked eye. A new fixative was added, and the cells were transferred to 4°C. The fixative was then aspirated and fixed with pre-chilled 1% osmium acid-0.1 M phosphate buffer (pH 7.4) at RT for 2 h. Samples were then dehydrated in increasing ethanol solutions (50%, 70%, 80%, 90%, 95%, and 100%). The samples were permeabilized overnight using an acetone:812 embedding agent (1:1) mixture. Pure 812 embedding agent (SPI, 90529-77-4) was permeated overnight. Finally, embedding sections, uranium-lead double staining, and cell morphology were observed under transmission electron microscopy (FEI, USA). PBS was used for all washing steps.

Growth assay and doubling time

The cells were inoculated in 96-well plates at a density of 10^5 cells/mL, and each well was inoculated with 100 μ l of cell suspension and incubated at 37°C in a 5% CO₂ incubator. Five wells were taken every 24 h to aspirate and discard the original complete medium, add the configured Cell Counting Kit-8 (CCK-8) solution (hycezmio, Wuhan, China), and incubate for 1 h with protection from light. CCK-8 solution was diluted with DMEM at a ratio of 10:1. The OD value of each well was measured at 450 nm for 6–8 consecutive d until the cells entered the plateau phase. The cell growth curve was established using the standard curve of the cell assay with a known OD value, and the multiplication time was calculated based on the regression equation of the curve using GraphPad Prism 9 software.

Single-cell cloning

Cells in good growth conditions were counted and inoculated in 6-well plates at a density of 100 cells per well and then gently shaken in a cross direction to disperse the cells evenly. The 6-well plates were transferred to a 37°C incubator for 2–3 weeks, and the medium was changed at the appropriate time. When clones visible to the naked eye appeared, the culture was harvested, after which the culture medium was discarded, and the cells were washed carefully with PBS twice. Then, 2 mL of methanol fixative was added to each well and incubated for 30 min. The cells were stained with 0.1% crystalline violet staining solution (BKMAM, BKMAM Biotechnology) for 25 min, after which the staining solution was washed off slowly with running water, and the fixed cells were air dried. After that, the number of clones with more than 50 cells was counted under a microscope, and the cloning efficiency of cells was calculated according to the formula:

Cytogenetic analysis

For karyotype analysis, cells in the growth phase were treated with 0.05 mg/mL colchicine for 5 h. Then, adherent cells were dissociated with 0.25% trypsin and resuspended in 0.075 M hypotonic KCl (preheated to 37°C) for 30 min at 37°C. The cell suspension was then fixed in methanol: acetic acid (3:1) and added dropwise to clean and cold slides. Finally, the prepared slides were stained with Giemsa (Sigma, Aldrich) for 15 min, and the chromosome numbers of the cells were counted in 50 metaphase cells. The chromosomes were observed and counted under an optical microscope (Olympus, Japan).

Cell-specific staining

Alizarin red staining. The cells were spread in the crawling slices of six-well plates, grown to 80–90% confluence, washed with PBS, fixed with 4% paraformaldehyde for 20 min, stained with 0.1% alizarin red-Tris-HCl (pH 4.2) solution for 30 min, washed with distilled water, removed the crawling slices, dried, sealed, and observed under the microscope.

Toluidine blue staining. The cells were spread in the crawling slices of six-well plates, grown to 80–90% confluence, discarded from the medium, washed with PBS, fixed with 4% paraformaldehyde for 20 min, stained with toluidine blue staining solution for 30 min, then washed with PBS to remove the excess staining solution, removed the crawling slices, dried, sealed, and observed under the microscope.

Histological and immunohistochemistry analyses

Tissues were fixed in 4% formaldehyde solution, paraffin-embedded, and sections were stained with H&E. IHC detection using antibodies specific for BGLAP (ABclonal, Ab-A14636), SPARC (ABclonal, Ab-A1615), ALPL (ABclonal, Ab-A1080), CGA (GeneTech, GT2114), S100 (GeneTech, GZ0311), VIM (Boster, BM0135), PCK (Boster, BM0030) and CD31 (GeneTech, MB-1) was performed on paraffin sections. In this detection, those without primary antibodies were negative controls. Cross-reactivity of primary antibodies with canine tissues involved in IHC and IF has been previously demonstrated. The staining processes were performed according to standard methods. The sections were observed using an optical microscope (Olympus, Japan).

Immunofluorescence staining

An indirect IF assay detected the expression of BGLAP, SPARC, ALPL, CGA, S100, VIM, PCK, and CD31 in the Mango cell line. Cells growing on 12-well plates were fixed with 4% paraformaldehyde for 30 min. Cells were incubated with primary antibodies overnight at 4°C and without primary antibodies as a negative control. The next day, the cells were washed and incubated with Alexa Fluor 594 goat anti-rabbit IgG (Affinity Biosciences, S0001) as a secondary antibody for 1 h at RT. The cells were washed and stained with DAPI (Beyotime, China). Then, the cells were examined under a fluorescence microscope (Olympus, Japan). PBS was used for all washing steps.

Tumorigenicity in nude mice

Five-week-old BALB/C nude male mice were purchased from the Hubei Provincial Center for Experimental Animal Research (Wuhan, China). Mice were maintained under free diet conditions in a room with their temperature at 25 °C. The mice were used to investigate the tumorigenicity of the Mango cell line at passage 20. A suspension of 5×10^6 cells in 0.2 mL PBS was transplanted subcutaneously into the dorsal region of mice ($n=5$). The mice were inspected for tumor development every 2–3 d. When tumors were detected, they were monitored by palpation and measured by calipers every 2–3 d. Mice were euthanized 23 d after inoculation by cervical dislocation and autopsied to detect metastatic lesions in the lungs or other organs. Tumors and organs were collected at necropsy and placed in 4% paraformaldehyde (pH=7.4) for histological and IHC examinations.

Abbreviations

ALPL	Alkaline phosphatase
BGLAP	Bone gamma-carboxyglutamate protein
CCK-8	Cell Counting Kit-8
CGA	Chromogranin A
CSA	Chondrosarcoma

CT	Computed tomography
DMEM	Dulbecco's modified Eagle's medium
FBS	Fetal bovine serum
FNA	Fine-needle Aspiration
HBSS	Hanks' Balanced Salt Solution
H&E	Hematoxylin-eosin
IF	Immunofluorescence
IHC	Immunohistochemistry
MRI	Magnetic resonance imaging
OSA	Osteosarcoma
PBS	Phosphate-buffered saline
PCK	Pan cytokeratin
RT	Room temperature
SPARC	Secreted protein acidic and rich in cysteine
VIM	Vimentin
VSSO	Veterinary Society for Surgical Oncology

Acknowledgements

We thank all Laboratory of Veterinary Clinical Diagnosis members for helpful discussions and suggestions.

Authors' contributions

MW, XW, HG and CQ conceived and designed the experiments, respectively. MW, HG and CQ performed the experiments and data analysis. LH, XW, WL, QZ, WZ, HF, CL, BZ took part some of the experiments. MW composed most of the manuscript. Figures were produced by MW, LH, XW and CQ. Critical revisions were made by CQ. All authors have read and approved the final manuscript.

Funding

This study was supported by the National Natural Science Foundation of China (Grant Number: 32172925).

Availability of data and materials

The original contributions presented in the study are included in the article. Further inquiries can be directed to the corresponding authors.

Declarations

Ethics approval and consent to participate

The animal study was reviewed and approved by all animal procedures, and the study design was approved by the animal ethics committee of Huazhong Agricultural University. Ethics number: HZAUMO-2023-0058.

Consent for publication

Not applicable.

Competing interests

The authors declare that the research was conducted in the absence of any commercial or financial relationships that could be construed as a potential conflict of interest.

Received: 22 April 2023 Accepted: 29 July 2023

Published online: 08 September 2023

References

- Al-Khan, A.A., H.J. Gunn, M.J. Day, M. Tayebi, S.D. Ryan, C.A. Kuntz, E.S. Saad, S.J. Richardson, and J.A. Danks. 2017. Immunohistochemical validation of spontaneously arising canine osteosarcoma as a model for human osteosarcoma. *Journal of Comparative Pathology* 157: 256–265. <https://doi.org/10.1016/j.jcpa.2017.07.005>.
- Amaral, C.B., J.D.S. Leite, A.B.M. Fonseca, and A.M.R. Ferreira. 2018. Vimentin, osteocalcin and osteonectin expression in canine primary bone tumors: Diagnostic and prognostic implications. *Molecular Biology Reports* 45: 1289–1296. <https://doi.org/10.1007/s11033-018-4285-6>.
- Chikata, S., S. Nakamura, R. Katayama, S. Yanagisawa, Y. Matsuo, I. Yamane, and K. Takahashi. 2006. Primary chondrosarcoma in the liver of a dog. *Veterinary Pathology* 43: 1033. <https://doi.org/10.1354/vp.43-6-1033>.

- Davis, G.J., A.S. Kapatkin, L.E. Craig, G.S. Heins, and J.A. Wortman. 2002. Comparison of radiography, computed tomography, and magnetic resonance imaging for evaluation of appendicular osteosarcoma in dogs. *Journal of the American Veterinary Medical Association* 220: 1171–1176. <https://doi.org/10.2460/javma.2002.220.1171>.
- Engel, H., G.W. Herget, H. Füllgraf, R. Sutter, M. Benndorf, F. Bamberg, and P.M. Jungmann. 2021. Chondrogenic bone tumors: The importance of imaging characteristics. *Rofo* 193: 262–275. <https://doi.org/10.1055/a-1288-1209>.
- Fanburg, J.C., A.E. Rosenberg, D.L. Weaver, K.O. Leslie, K.G. Mann, D.J. Taatjes, and R.P. Tracy. 1997. Osteocalcin and osteonectin immunoreactivity in the diagnosis of osteosarcoma. *American Journal of Clinical Pathology* 108: 464–473. <https://doi.org/10.1093/ajcp/108.4.464>.
- Farese, J.P., J. Kirpensteijn, M. Kik, N.J. Bacon, S.S. Waltman, B. Seguin, M. Kent, J. Liptak, R. Straw, M.N. Chang, Y. Jiang, and S.J. Withrow. 2009. Biologic behavior and clinical outcome of 25 dogs with canine appendicular chondrosarcoma treated by amputation: A Veterinary Society of Surgical Oncology retrospective study. *Veterinary Surgery* 38: 914–919. <https://doi.org/10.1111/j.1532-950X.2009.00606.x>.
- Gelderblom, H., P.C.W. Hogendoorn, S.D. Dijkstra, C.S. van Rijswijk, A.D. Krol, A.H.M. Taminiau, and J.V.M.G. Bovée. 2008. The clinical approach towards chondrosarcoma. *The Oncologist* 13: 320–329. <https://doi.org/10.1634/theoncologist.2007-0237>.
- Kim, M.J., K.J. Cho, A.G. Ayala, and J.Y. Ro. 2011. Chondrosarcoma: With updates on molecular genetics. *Sarcoma* 2011: 405437. <https://doi.org/10.1155/2011/405437>.
- Kito, F., R. Oyama, M. Sakumoto, M. Takahashi, K. Shiozawa, Z. Qiao, H. Sakamoto, T. Hirose, N. Setsu, A. Yoshida, A. Kawai, and T. Kondo. 2018. Establishment and characterization of novel patient-derived osteosarcoma xenograft and cell line. *In Vitro Cellular & Developmental Biology-Animal* 54: 528–536. <https://doi.org/10.1007/s11626-018-0274-2>.
- Lee, J.S., and C.-H. Tung. 2013. Osteotropic cancer diagnosis by an osteocalcin inspired molecular imaging mimetic. *Biochimica et Biophysica Acta (BBA)-General Subjects* 1830: 4621–4627. <https://doi.org/10.1016/j.bbagen.2013.05.015>.
- Liao, Y.-X., Y.-Q. Hua, and Z.-D. Cai. 2013. Current advances in animal model of chondrosarcoma and related research. *Biomedical Reports* 1: 3–6. <https://doi.org/10.3892/br.2012.13>.
- Liu, Y., X. Feng, Y. Zhang, H. Jiang, X. Cai, X. Yan, Z. Huang, F. Mo, W. Yang, C. Yang, S. Yang, and X. Liu. 2016. Establishment and characterization of a novel osteosarcoma cell line: CHOS. *Journal of Orthopaedic Research* 34: 2116–2125. <https://doi.org/10.1002/jor.23245>.
- Madarama, H., H. Itoh, S. Yoshida, I. Sakonju, K. Takase, and Y. Hasegawa. 1998. Canine mesenchymal chondrosarcoma of the ribs. *Journal of Veterinary Medical Science* 60: 975–979. <https://doi.org/10.1292/jvms.60.975>.
- Meyer, F.R.L., and I. Walter. 2016. Establishment and characterization of new canine and feline osteosarcoma primary cell lines. *Veterinary Sciences* 3: 9. <https://doi.org/10.3390/vetsci3020009>.
- Miwa, S., N. Yamamoto, K. Hayashi, A. Takeuchi, K. Igarashi, and H. Tsuchiya. 2022. Therapeutic targets and emerging treatments in advanced chondrosarcoma. *International Journal of Molecular Sciences* 23: 1096. <https://doi.org/10.3390/ijms23031096>.
- Monderer, D., A. Luseau, A. Bellec, E. David, S. Ponsolle, S. Saiagh, S. Bercegeay, P. Piloquet, M.G. Denis, L. Lodé, F. Rédini, M. Biger, D. Heymann, M.-F. Heymann, R. Le Bot, F. Gouin, and F. Blanchard. 2013. New chondrosarcoma cell lines and mouse models to study the link between chondrogenesis and chemoresistance. *Laboratory Investigation* 93: 1100–1114. <https://doi.org/10.1038/labinvest.2013.101>.
- Montinaro, V., S.E. Boston, P. Buracco, W.T.N. Culp, G. Romanelli, R. Straw, and S. Ryan. 2013. Clinical outcome of 42 dogs with scapular tumors treated by scapulectomy: A Veterinary Society of Surgical Oncology (VSSO) retrospective study (1995–2010). *Veterinary Surgery* 42: 943–950. <https://doi.org/10.1111/j.1532-950X.2013.12066.x>.
- Morello, E., M. Martano, and P. Buracco. 2011. Biology, diagnosis and treatment of canine appendicular osteosarcoma: similarities and differences with human osteosarcoma. *The Veterinary Journal* 189: 268–277. <https://doi.org/10.1016/j.tvjl.2010.08.014>.
- Poon, A.C., A. Matsuyama, and A.J. Mutsaers. 2020. Recent and current clinical trials in canine appendicular osteosarcoma. *The Canadian Veterinary Journal* 61: 301–308. PMID: 32165755 and PMID: PMC7020630.
- Rizzo, V.L., C.B. Levine, and J.J. Wakshlag. 2017. The effects of sulforaphane on canine osteosarcoma proliferation and invasion. *Veterinary and Comparative Oncology* 15: 718–730. <https://doi.org/10.1111/vco.12212>.
- Séguin, B., T. Zwerdling, J.L. McCallan, H.E.V. DeCock, L.L. Dewe, D.K. Naydan, A.E. Young, D.L. Bannasch, O. Foreman, and M.S. Kent. 2006. Development of a new canine osteosarcoma cell line. *Veterinary and Comparative Oncology* 4: 232–240. <https://doi.org/10.1111/j.1476-5829.2006.00112.x>.
- Tlemsani, C., F. Larousserie, S. De Percin, V. Audard, D. Hadjadj, J. Chen, D. Biau, P. Anract, B. Terris, F. Goldwasser, E. Pasmant, and P. Boudou-Rouquette. 2023. Biology and management of high-grade chondrosarcoma: An update on targets and treatment options. *International Journal of Molecular Sciences* 24: 1361. <https://doi.org/10.3390/ijms24021361>.
- T-raylor, J.I., M.N. Pernik, A.R. Plitt, M. Lim, and T. Garzon-Muvdi. 2021. Immunotherapy for chordoma and chondrosarcoma: Current evidence. *Cancers (Basel)* 13 (10): 2408. <https://doi.org/10.3390/cancers13102408>.
- Van Oosterwijk, J.G., J.K. Anninga, H. Gelderblom, A.-M. Cleton-Jansen, and J.V.M.G. Bovée. 2013. Update on targets and novel treatment options for high-grade osteosarcoma and chondrosarcoma. *Hematology/Oncology Clinics of North America, Sarcoma* 27: 1021–1048. <https://doi.org/10.1016/j.hoc.2013.07.012>.
- Vanel, M., L. Blond, and D. Vanel. 2013. Imaging of primary bone tumors in veterinary medicine: Which differences? *European Journal of Radiology* 82: 2129–2139. <https://doi.org/10.1016/j.ejrad.2011.11.032>.
- Vinayak, A., D.R. Worley, S.J. Withrow, D.S. Adams, and B.E. Powers. 2018. Dedifferentiated chondrosarcoma in the dog and cat: A case series and review of the literature. *Journal of the American Animal Hospital Association* 54: 50–59. <https://doi.org/10.5326/JAAHA-MS-6566>.
- Wehrle-Martinez, A.S., K.E. Dittmer, D. Aberdein, and K.G. Thompson. 2016. Osteocalcin and osteonectin expression in canine osteosarcoma. *Veterinary Pathology* 53: 781–787. <https://doi.org/10.1177/0300985815626574>.
- Whelan, J.S., and L.E. Davis. 2018. Osteosarcoma, chondrosarcoma, and chordoma. *Journal of Clinical Oncology* 36: 188–193. <https://doi.org/10.1200/JCO.2017.75.1743>.
- Zu, L., X. Li, J. He, N. Zhou, F. Meng, Xiaozhou Li, S. Xu, and L. Zhang. 2022. Establishment and characterization of a novel highly malignant lung cancer cell line ZX2021H derived from a metastatic lymph node lesion. *Thoracic Cancer* 13: 1199–1210. <https://doi.org/10.1111/1759-7714.14385>.

Publisher's Note

Springer Nature remains neutral with regard to jurisdictional claims in published maps and institutional affiliations.

Ready to submit your research? Choose BMC and benefit from:

- fast, convenient online submission
- thorough peer review by experienced researchers in your field
- rapid publication on acceptance
- support for research data, including large and complex data types
- gold Open Access which fosters wider collaboration and increased citations
- maximum visibility for your research: over 100M website views per year

At BMC, research is always in progress.

Learn more biomedcentral.com/submissions

